New proton conducting membranes with high retention of protic ionic liquids

ARTICLE *in* JOURNAL OF MATERIALS CHEMISTRY · FEBRUARY 2011

Impact Factor: 7.44 · DOI: 10.1039/C0JM02878A

8 AUTHORS, INCLUDING:

Yun sheng Ye
Huazhong University of Science and Technol…
48 PUBLICATIONS **664** CITATIONS
SEE PROFILE

Bing Joe Hwang
National Taiwan University of Science and T…
320 PUBLICATIONS **6,121** CITATIONS
SEE PROFILE

THE JOURNAL OF PHYSICAL CHEMISTRY C

ARTICLE

pubs.acs.org/JPCC

Nanoscale Correlation between Exciton Dissociation and Carrier Transport in Silole-Containing Cyclopentadithiophene-Based Bulk Heterojunction Films

Jen-Hsien Huang,[†] Chin-Min Teng,[‡] Yu-Sheng Hsiao,[†] Feng-Wen Yen,[‡] Peilin Chen,[†] Feng-Chih Chang,[§] and Chih-Wei Chu[†,∥,*]

[†]Research Center for Applied Sciences, Academia Sinica, Taipei, Taiwan 11529,

[‡]Luminescence Technology Corporation, Hsinchu, Taiwan 300,

[§]Department of Applied Chemistry and [∥]Department of Photonics, National Chiao-Tung University, Hsinchu, Taiwan 30010

ABSTRACT: Understanding the effects of conjugated polymer structures on exciton lifetimes and morphologies within bulk heterojunction (BHJ) films is a necessary step toward the development of better organic solar cells. Studying the impact of a polymer's structure on the optical, morphological, and performance characteristics of a device can lead to advances in the design of new polymers. In this study, we synthesized carbon- and silicon-bridged cyclopentadithiophene- (CPDT-) based polymers and determined their photophysical properties and morphologies by measuring the exciton lifetime distributions in their BHJ films. The silicon-bridged CPDT-based polymer/[6,6]-phenyl-C_{61}-butyric acid methyl ester (PCBM) BHJ exhibited a higher degree of luminescence quenching, suggesting that thermodynamically favorable mixing on the molecular scale and nanoscale phase separation occurred simultaneously in the blend film. We attribute this favorable morphology to the presence of strong $\pi-\pi$ stacking in the silicon-bridged CPDT-based polymers. Under AM 1.5 G illumination (100 mA cm^{-2}), a device incorporating the silicon-bridged CPDT-based polymer and PCBM (1:2, w/w) gave an overall power conversion efficiency of 3.5% with a short-circuit current of 9.0 mA cm^{-2}, an open-circuit voltage of 0.72 V, and a fill factor of 53.6%.

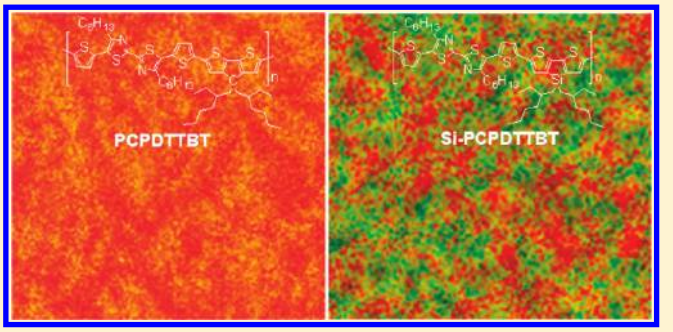

INTRODUCTION

Polymer solar cells have attracted much scientific interest because of their potential to reduce fabrication costs by taking advantage of solution-deposition methods and high stability compared with dye-sensitized solar cells.[1−5] One of the important factors affecting the power conversion efficiency (PCE) in polymer solar cells is the morphology of the BHJ films. The ideal morphology would feature (i) a high level of mixing between donors and acceptors, to create a large interfacial surface area that allows exciton dissociation, and (ii) percolating pathways across the film for the transport of photogenerated electrons and holes.[6−9] A number of methods, including thermal annealing,[10−13] solvent annealing,[14−17] and the use of processing additives,[18−21] have been proposed to efficiently modulate polymer film morphology on the nanoscale. Thermal and solvent annealing can induce the self-organization of conjugated polymers, leading to stronger interchain interactions. A recently developed mixed-solvent approach involves the addition of alkanedithiols into the solvent used to fabricate the solar cell devices. These alkanedithiols selectively dissolve [6,6]-phenyl-C_{61}-butyric acid methyl ester (PCBM), but not poly(3-hexylthiophene) (P3HT) or any of the other polymers used. This method allows efficient phase separation to occur during the drying process, leading to favorable morphologies for the transport of the carriers to their respective electrodes.

In addition to the approaches mentioned above, the use of silole-containing polymers is another promising method for controlling film morphology and improving device performance. Many groups have reported that replacing a carbon atom with a silicon atom on the main chain of a conjugated polymer can led to increases in solar cell efficiency.[22,23] Scharber et al.[24] and Chen et al.[25] reported that replacing the bridge carbon atom in cyclopentadithiophene- (CPDT-) based polymers with a silicon atom leads to films exhibiting greater crystallinity. These silole-containing polymers feature slightly distorted CPDT units relative to those of their carbon-bridged congeners. The longer Si−C bond[25] modifies the geometry of the fused dithophene unit, resulting in better ordering of the polymer chains and, consequently, better charge-transport properties. Because the photocurrent in a polymer solar cell is proportional to the product of the photocarrier density generation rate and the carrier mobility,[6] improved charge transport has an entirely positive effect on solar cell efficiency. The dissociation of electron/hole pairs at the donor−acceptor interface is, however, an important process that limits the charge-generation efficiency under normal operation

Received: September 23, 2010
Revised: December 1, 2010
Published: January 5, 2011

conditions; this phenomenon can be measured in terms of the exciton lifetime. The relationship between the chemical structure of a conjugated polymer and the exciton lifetime remains poorly understood, even though these two properties are the most fundamental characteristics directly influencing cell performance. In this study, we synthesized a CPDT-based copolymer (PCPDTTBT) and its silole-based derivative, poly[(4,4′-bis-(2-ethylhexyl)dithieno[3,2-b:2′,3′-d]silole)-2,6-diyl-*alt*-(5,5′-thienyl-4,4′-dihexyl-2,2′-bithiazole)-2,6-diyl] (Si-PCPDTTBT). We then combined confocal optical microscopy with a time-resolved detection module to investigate the relationship between the morphologies of the resulting blend films and the exciton lifetimes.[26,27] The time- and spatial-domain signals revealed the effects of the different bridging atoms in the CPDT units on the exciton dissociation and carrier transport within bulk heterojunction (BHJ) films on the nanoscale.

RESULTS AND DISCUSSION

We synthesized PSPDTTBT according to literature procedures.[28] The bithiazole-based monomer **5** was prepared from 1-bromo-2-octanone (**1**) using Stille and Suzuki coupling reactions (Scheme 1). The synthetic routes of the silicon-bridged CPDT unit (**11**) are shown Scheme 2. As shown in Scheme 3, further coupling of monomers **5** and **11** successfully resulted in the Si-PCPDTTBT copolymer. All precursors were satisfactorily characterized using ^{1}H NMR spectroscopy and mass spectrometry. The two pendent 2-ethylhexyl side chains on the Si-CPDT units and the one long hexyl chain on the bithiazole units enhanced the solubilities and the solution processabilities/tractabilities of the polymers. The copolymers were completely soluble in the organic solvents chloroform, tetrahydrofuran (THF), and chlorobenzene at room temperature.

Scheme 1. Synthetic Pathways of Bithiazole-Based Monomers

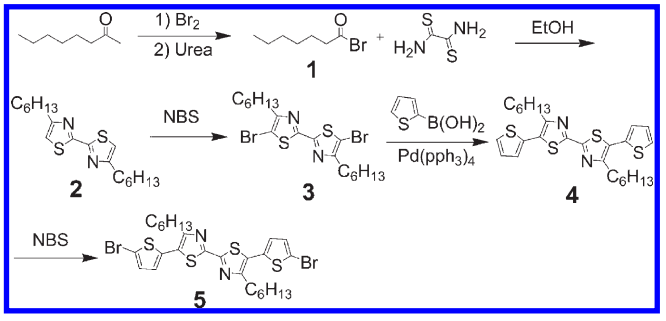

Scheme 2. Synthetic Route toward Silicon-Bridged CPDT

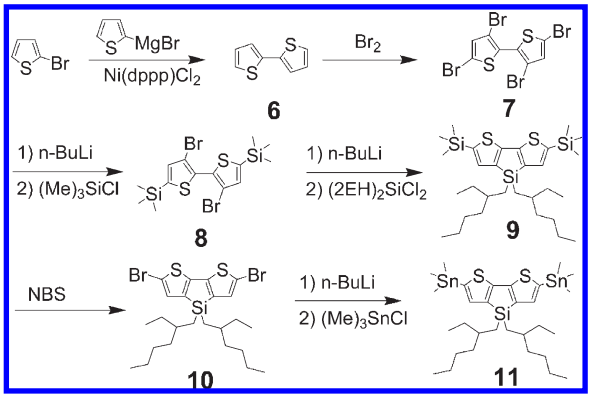

Figure 1 presents cyclic voltammograms of PCPDTTBT and Si-PCPDTTBT cast on a platinum disk electrode in 0.1 M $TBAPF_6$/MeCN; the electrochemical behaviors of PCPDTTBT and Si-PCPDTTBT were almost identical. Using the onset oxidation and reduction potentials obtained from the cyclic voltammograms,[29] we estimate the highest occupied molecular orbital (HOMO) and lowest unoccupied molecular orbital (LUMO) levels to be 5.10 and 3.55 eV, respectively, for both PCPDTTBT and Si-PCPDTTBT.

Figure 2 presents normalized absorbance and photoluminescence (PL) spectra of the carbon- and silicon-bridged polymers. The absorbance spectrum of PCPDTTBT reveals a broad featureless absorption peak located at 530 nm. Notably, the absorbance spectrum of Si-PCPDTTBT displays a markedly red-shifted absorption (560 nm) relative to that of PCPDTTBT and a pronounced vibronic peak at 610 nm. These features indicate that the silole ring enhances the conjugation and interactions of the polymer chains.[30] Chen et al. have developed a computational method for simulating silole-containing polymers. They claimed that the C−Si bond is significantly longer than the C−C bond, which reduces the steric hindrance from the bulky alkyl groups. As a result, the polymer changes from an amorphous (carbon-based polymer) to a highly crystalline (silicon-based polymer) structure, which leads to the red shift and the vibronic peak of absorbance.[25] The PL spectra reveal very similar behavior, with a PL emission maximum centered at 710 nm for each polymer. However, the PL spectrum of Si-PCPDTTBT is red-shifted and shows a long-lived component compared with the carbon counterpart. The observed long-lived component indicates that a charge-transfer state is active in this system induced by an increase in $\pi-\pi$ interaction and hence electronic delocalization.[31,32] This can lead to favorable consequences for solar-cell performance.

For a BHJ solar cell to achieve high efficiency, it requires a well-mixed domain of donor and acceptor units and the presence of percolating pathways for charge transport. Although it can be difficult to measure the degree of mixing of a bicomponent phase and its morphology simultaneously, in this study, we measured the exciton lifetime distributions (ELDs) of the blended films to obtain both types of information at the same time. Figure 3 presents scanning confocal ELD images of PCPDTTBT/PCBM and Si-PCPDTTBT/PCBM (1:1, wt %) films. The ELD images were measured after excitation at 470 nm using a picosecond laser microscope (resolution: 512 × 512 pixels). The exciton lifetimes were satisfactorily fitted using a multiexponential

Scheme 3. Synthetic Route of Si-PCPDTTBT Copolymer

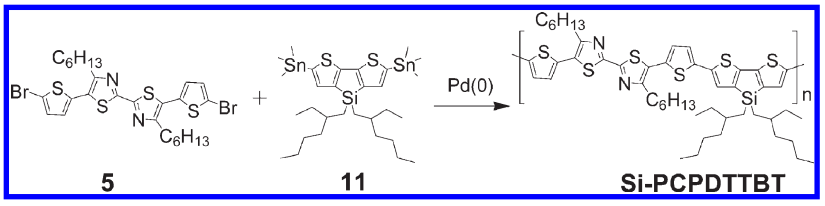

dx.doi.org/10.1021/jp1090894 |J. Phys. Chem. C 2011, 115, 2398–2405

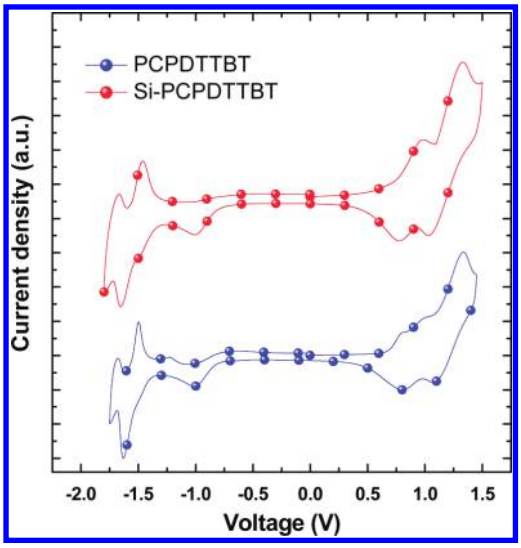

Figure 1. Cyclic voltammograms of the PCPDTTBT and Si-PCPDTTBT films.

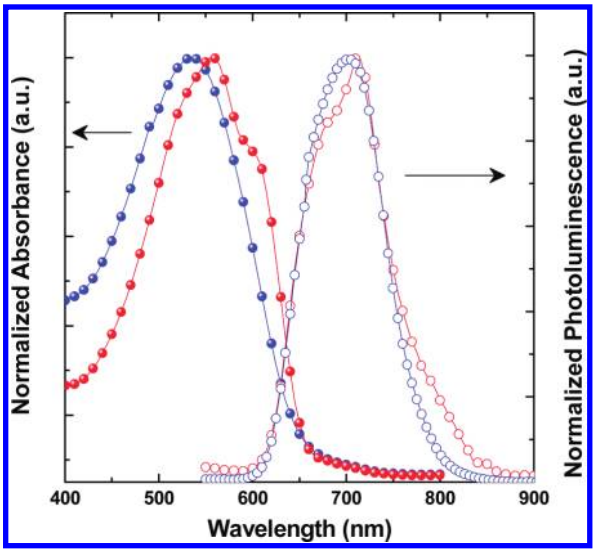

Figure 2. Normalized absorbance and PL spectra of the PCPDTTBT (blue) and Si-PCPDTTBT (red) polymer films.

model.[32] These extracted values allowed us to construct two-dimensional exciton lifetime images. From the 10 × 10 μm ELD images of the PCPDTTBT/PCBM and Si-PCPDTTBT/PCBM blending films, the constructed lifetime images reveal that both contained almost-homogeneous phases. Nevertheless, the PCPDTTBT/PCBM film provided a longer exciton lifetime than the Si-PCPDTTBT/PCBM film, suggesting that the degree of exciton dissociation was greater for the Si-PCPDTTBT/PCBM film, leading to its larger photogeneration efficiency. These conclusions are further supported by the transmitted images in Figure 3c,d. The Si-PCPDTTBT/PCBM film provided a lower PL emission intensity in the overall film relative to that of the PCPDTTBT/PCBM film. This behavior suggests that good mixing exists between the polymer and the fullerene, leading to more-efficient energy transfer. Close scrutiny reveals some red spots (regions of longer exciton lifetime) in Figure 3b. From comparison with the transmitted images, the red spots represent

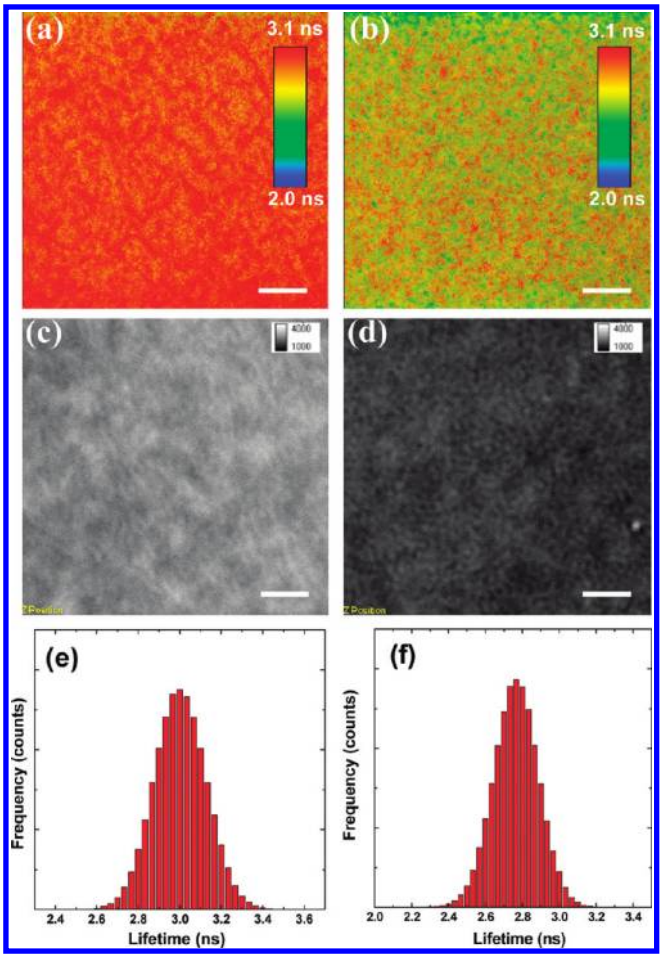

Figure 3. (a,b) Exciton lifetimes, (c,d) transmitted images, and (e,f) histograms of the exciton lifetimes for the (a,c,e) PCPDTTBT/PCBM and (b,d,f) Si-PCPDTTBT/PCBM blend films, measured after excitation at 470 nm using a picosecond laser microscope (512 × 512 pixels). Scale bars: 2 μm.

higher levels of PL emission; presumably, they arose from the aggregation of polymer chains. To quantify the variations in PL quenching, we fitted the resulting ELD images with a Gaussian function (Figure 3e,f), obtaining average lifetimes for PCPDTTBT/PCBM and Si-PCPDTTBT/PCBM of 3.11 and 2.66 ns, respectively, over lifetime distributions ranging from 2.62 to 3.35 ns and from 2.20 to 2.93 ns, respectively. The PL quenching phenomena presumably arose through rapid energy or electron transfer to PCBM. The variations in the exciton lifetimes indicate the presence of compositional separation within the blended films.

The photophysical properties of a blend film are the most fundamental characteristics directly influencing cell performance. Unfortunately, the resolution of confocal optical microscopy is restricted by the applied laser wavelength, which is typically 400−500 nm. To gain insight into the nanostructure within the films, Sauer and co-workers used confocal fluorescence lifetime imaging microscopy to measure the distance between two dye molecules that were less than 30 nm apart.[33] They demonstrated that ultra-high-resolution imaging can be established by combining the spatial- and time-domain signals from confocal microscopy and fluorescence lifetime measurements. In this study, we applied their technique to correlate the chemical structure with the photophysical properties on the

nanoscale. Figure 4 presents expanded views of the lifetime images of the blended films. Because the color contrast of the Si-PCPDTTBT/PCBM film is much greater than that of the PCPDTTBT/PCBM film, its degree of phase separation is also greater. The image of Si-PCPDTTBT/PCBM film features an extensive red, yellow, and green network related to low-, moderate-, and high-level quenching, respectively. We assign the yellow region to a well-mixed zone of polymer and PCBM, with a feature size of 30−50 nm, and the red and green regions to polymer- and PCBM-rich regions, respectively. The yellow region features a large interface for excitons to dissociate into holes and electrons, which can then be transported through the polymer- and PCBM-rich channels to their related electrodes. In contrast, the image for the PCPDTTBT/PCBM blend lacks the "green" channel for transport of the charge carriers. Based on these results, we conclude that the Si-PCPDTTBT/PCBM blend features not only large-scale phase separation for efficient charge transport but also better mixing, relative to that of the PCPDTTBT/PCBM blend, on the molecular scale for exciton dissociation.

Next, we used atomic force microscopy (AFM) and transmission electron microscopy (TEM) to analyze the correlation between the film morphology and the chemical structure. Figure 5 presents AFM images of the surface morphologies of two films that had been spin-cast onto indium tin oxide (ITO) substrates. These images are consistent with the ELD images in Figure 4. The PCPDTTBT/PCBM film features smooth and mixed domains that are amorphous in nature (Figure 5a). In contrast, the film of the Si-PCPDTTBT/PCBM blend exhibits coarse, chainlike features, having an average size of 30 nm, running across the surface (Figure 5b). The corresponding phase images in Figure 5c,d support these characterizations. The Si-PCPDTTBT/PCBM blend features many channels distributed throughout the film. Because phase contrast is related to differences in the mechanical properties (adhesion and stiffness) of materials, the image indicates that the peaks and valleys have different chemical characteristics, consistent with polymer- and PCBM-rich domains that can promote charge transport, as in Figure 4.

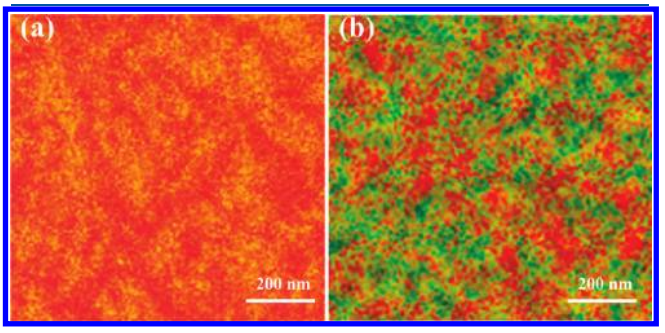

Figure 4. Exciton lifetime images of (a) PCPDTTBT/PCBM and (b) Si-PCPDTTBT/PCBM blend films. Scale bars: 200 nm.

We used TEM to investigate the morphologies of thin free-standing films of PCPDTTBT/PCBM and Si-PCPDTTBT/PCBM blend films. All samples were spin-cast from 1,2-dichlorobenzene onto 30-nm-thick poly(3,4-ethylenedioxythiophene): poly(styrene sulfonate) (PEDOT:PSS). The darker regions in Figure 6 represent nanocrystalline PCBM domains having electron density higher than that of the polymer. Again, the introduction of the silicon bridge induced a larger degree of phase separation between the polymer and the fullerene, relative to that of the carbon counterpart. The introduction of the silicon atom led to an increase in crystallinity, mainly for the polymer phase, but also for the PCBM.[34,35] Much coarser and longer Si-PCPDTTBT crystals, having a characteristic feature size of approximately 20−30 nm, were formed through the stacking of several fine fibrillar Si-PCPDTTBT units. The degree of demixing of the two components increased, but large-scale phase separation did not occur, resulting in an interpenetrating network of both the polymer and the fullerene within the film. As a result of the expansion of the crystalline domains, we would

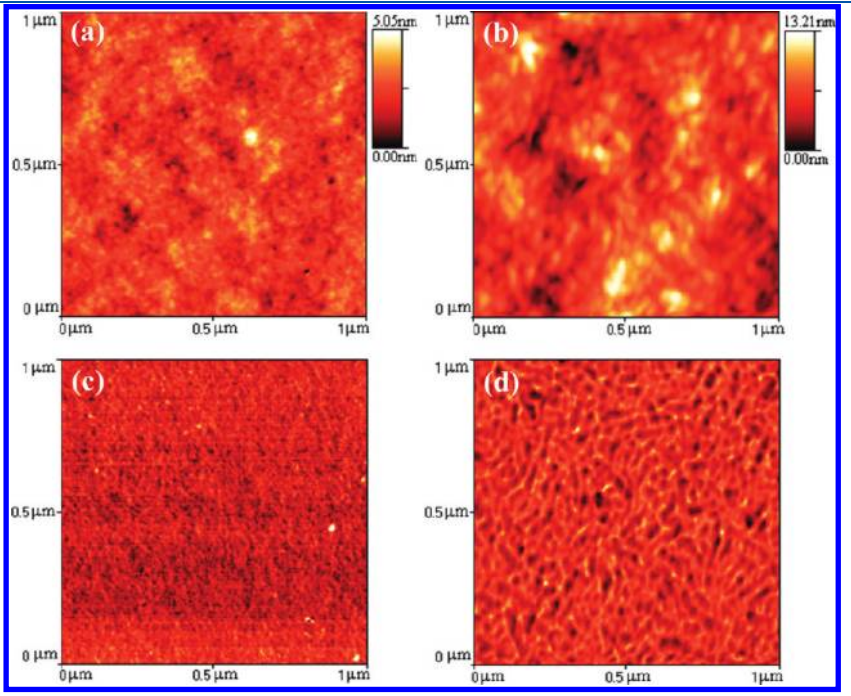

Figure 5. AFM (a,b) height and (c,d) phase images of the (a,c) PCPDTTBT/PCBM and (b,d) Si-PCPDTTBT/PCBM blend films.

dx.doi.org/10.1021/jp1090894 |J. Phys. Chem. C 2011, 115, 2398–2405

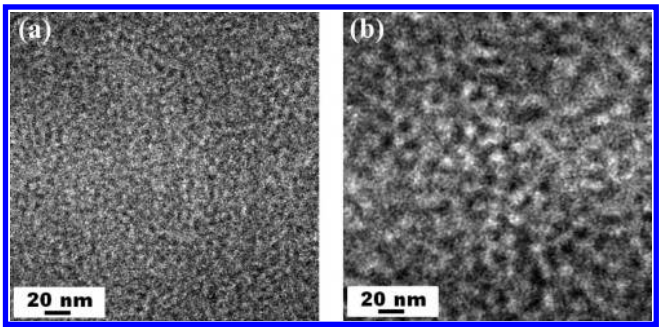

Figure 6. TEM images of the (a) PCPDTTBT/PCBM and (b) Si-PCPDTTBT/PCBM blend films.

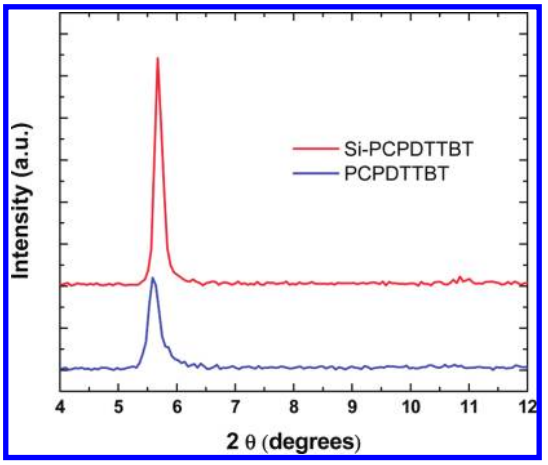

Figure 7. GIXRD spectra of the PCPDTTBT/PCBM and Si-PCPDTTBT/PCBM blend films.

expect the charge-transport properties to improve for both electrons and holes.[36,37]

To clarify the nature of the molecular stacking in the films of PCPDTTBT/PCBM and Si-PCPDTTBT/PCBM, we used grazing-incidence X-ray diffraction (GIXRD) to investigate their crystalline structures (see Figure 7). Both films exhibited an intense (100) diffraction peak, implying that they featured very highly ordered edge-on hexyl side chains. The much stronger peak intensity for Si-PCPDTTBT/PCBM is related to its greater film crystallinity. The 2θ angle of the maximum diffraction peak of the Si-PCPDTTBT/PCBM film (5.7°) was greater than that of the PCPDTTBT/PCBM film (5.6°). Substitution of these values into the Bragg equation yields a mean interlayer spacing for the Si-PCPDTTBT/PCBM film of 15.4 Å, which is 0.3 Å less than that of PCPDTTBT/PCBM film (15.7 Å). The presence of closer Si-PCPDTTBT chains suggests lower resistance to the hopping of carriers between Si-PCPDTTBT backbones.[38]

Figure 8 presents the current−voltage ($J-V$) curves and external quantum efficiencies (EQEs) of solar cells incorporating PCPDTTBT and Si-PCPDTTBT blended with PCBM. The Si-PCPDTTBT-based device provided a PCE of 3.3%, a short-circuit current density (J_{SC}) of 8.72 mA cm^{-2}, an open-circuit voltage (V_{OC}) of 0.74 V, and a fill factor (FF) of 51.1%. The performance of this device, with respect to the values of J_{SC} and FF, was an improvement over that of the solar cell prepared using the carbon-bridged analogue as the electron donor. The inset reveals that the spectral response of the Si-PCPDTTBT-based device featured contributions from the EQE in the wavelength range between 340

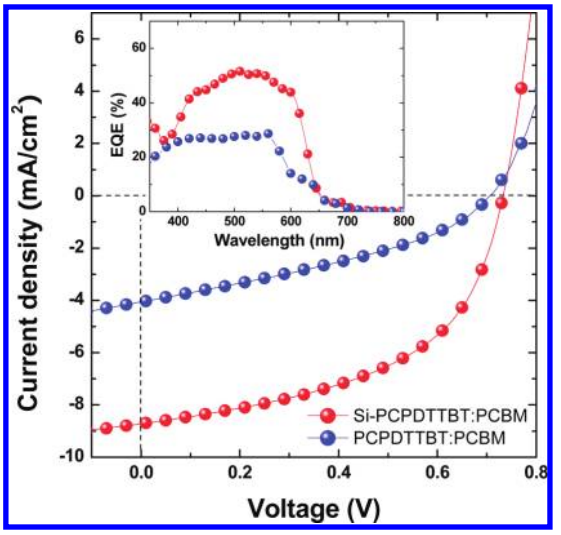

Figure 8. $J-V$ characteristics under illumination at 100 mW cm^{-2} (simulated AM 1.5G) of photovoltaic devices incorporating active layers based on PCPDTTBT and Si-PCPDTTBT. Inset: Corresponding EQE spectra of the devices.

and 710 nm. The maximum EQE for the PCPDTTBT-based device was 28% at a wavelength of 560 nm. In contrast, the Si-PCPDTTBT-based device provided an EQE maximum of ca. 50% at 560 nm. The significantly higher value of J_{SC} for the Si-PCPDTTBT-based device resulted from its more-favorable morphology, as evidenced by the superior quality of its percolating pathways and enhanced crystallinity in the exciton lifetime, AFM, and TEM images. We would expect that such a favorable morphology would promote charge transport, leading to higher values of J_{SC}. Table 1 summarizes the electron and hole mobilities calculated from the space-charge-limited current.[39,40] For the PCPDTTBT-based device, the electron (μ_e) and hole (μ_h) mobilities were 5.4×10^{-8} and 3.2×10^{-9} m^2 V^{-1} s^{-1}, respectively. For the Si-PCPDTTBT based device, the value of μ_e increased 5-fold to 2.7×10^{-7} m^2 V^{-1} s^{-1}, whereas that of μ_h increased by almost 2 orders of magnitude to 1.9×10^{-7} m^2 V^{-1} s^{-1}, resulting in highly balanced carrier transport ($\mu_e/\mu_h = 1.4$). The relatively small increase in electron mobility is understandable because the introduction of the silicon bridge resulted primarily in increased ordering of the polymer chains, a process that significantly affects hole mobility. The balanced carrier transport resulted from the formation of bicontinuous transport pathways within the entire active layer and the stronger crystallinity of the blend. Under these conditions, the current is not limited by space-charge effects, and high values of J_{SC} and FF are possible.

Highly ordered π-conjugated pathways benefit carrier mobility in polymer films. Recently, a "solvent annealing" approach was developed by Li et al.,[14,41] who found that self-organization in polymer chains was possible by controlling the polymer layer growth rate from the solution to the solid state. In the present study, we also investigated the effect of solvent annealing on the behavior of our silole-based polymer. Table 2 summarizes the performance of the cells incorporating PCPDTTBT and Si-PCPDTTBT, fabricated with and without solvent annealing. The values of both J_{SC} and FF were significantly dependent on the film growth rate for the PCPDTTBT/PCBM system. After solvent annealing had been performed, the values of J_{SC} and FF increased from 4.1 to 7.1 mA cm^{-2} and from 35.7 to 61.6%, respectively. With a value of V_{OC} of 0.7 V, this system provided a PCE of 3.05%, much greater than that obtained without solvent

Table 1. Photovoltaic Parameters and Mobilities for BHJ Devices Based on PCPDTTBT/PCBM and Si-PCPDTTBT/PCBM

sample	J_{SC} (mA cm^{-2})	V_{OC} (V)	FF (%)	PCE (%)	μ_e (m^2 V^{-1} s^{-1})	μ_h (m^2 V^{-1} s^{-1})	μ_e/μ_h
PCPDTTBT	4.1	0.71	35.7	1.04	5.4×10^{-8}	3.2×10^{-9}	16.9
Si-PCPDTTBT	8.7	0.73	51.9	3.33	2.7×10^{-7}	1.9×10^{-7}	1.4

Table 2. Photovoltaic Parameters for BHJ Devices Fabricated with and without Solvent Annealing

device condition	J_{SC} (mA cm^{-2})	V_{OC} (V)	FF (%)	PCE (%)
PCPDTTBT (fast-grown)[a]	4.1	0.71	35.7	1.04
PCPDTTBT (solvent-annealed)[b]	7.1	0.70	61.6	3.05
Si-PCPDTTBT (fast-grown)	8.7	0.73	51.9	3.33
Si-PCPDTTBT (solvent-annealed)	9.0	0.72	53.6	3.47

[a] Fast-grown devices were made by spin-coating the polymer/PCBM film until the film had dried. [b] Solvent-annealed devices were made according to the method reported in ref 14.

annealing. In contrast, the Si-PCPDTTBT/PCBM system delivered almost identical cell performance, regardless of the use or not of solvent annealing, suggesting that the introduction of the silicon bridge enhanced the degree of polymer stacking to achieve thermodynamic equilibrium. We suspect that the rapidly grown interpenetrating network constructed within the Si-PCPDTTBT/PCBM film achieved a favorable morphology that was very close to that established after solvent annealing of the PCPDTTBT/PCBM system.[23] Therefore, the cell featuring the Si-PCPDTTBT/PCBM film did not require solvent annealing to exhibit superior performance. Because solvent annealing consumes time and is not suitable for large-scale mass production, we believe that such silole-based polymers have great potential for industrial application.

CONCLUSIONS

We have synthesized a silole-containing low-bandgap polymer by replacing the C5 atom of PCPDTTBT with a silicon atom. From ELD images of the polymer/PCBM films, we found that the Si-PCPDTTBT/PCBM blends featured a higher degree of mixing between the polymer and the fullerene. Expanded ELD images also indicated that the Si-PCPDTTBT/PCBM blends underwent large-scale phase separation, with thermodynamically stable mixing on the nanoscale. As a result, this morphology of the Si-PCPDTTBT/PCBM blends enhanced both the rate of photocarrier generation and the charge-transport properties. The combination of these two effects enhanced the overall device efficiency. Thus, a subtle variation in monomer structure can influence material properties significantly, suggesting a direction for future polymer design.

EXPERIMENTAL SECTION

Measurement. ^{1}H NMR spectra were recorded using a Varian Unity 300 MHz spectrometer and $CDCl_3$ as the solvent. UV−vis absorption and PL spectra were recorded using HP G1103A and Hitachi F-4500 spectrophotometers, respectively. Cyclic voltammetry (CV) measurements were performed using a BAS 100 electrochemical analyzer and a standard three-electrode electrochemical cell, in 0.1 M $TBAPF_6$ (in MeCN) at room temperature with a scanning rate of 50 mV s^{-1}. For the fluorescence measurements, the samples were excited with light (wavelength: 470 nm) from a picosecond laser (LDH-P-C-470, PicoQuant); the fluorescence lifetime signal was measured using time-correlated single-photon counting (TCSPC). To map the lifetime images, the samples were scanned using an Olympus FV300 confocal optical microscope equipped with a PicoQuant PDM single-photon avalanche diode detector and a PicoQuant PicoHarp 300 USB interface for TCSPC. The fluorescence signal was improved using an edge filter (REF-473.0-25, CVI). The acquisition time for each lifetime image (pixel size: 512 × 512) was 20 min. The surface morphologies of the polymer films were investigated using an atomic force microscope (Digital Instrument NS 3a controller equipped with a D3100 stage). The EQE action spectra were obtained under short-circuit conditions. The light source was a 450-W Xe lamp (Oriel Instrument, model 6266) equipped with a water-based IR filter (Oriel Instrument, model 6123NS). The light output from the monochromator (Oriel Instrument, model 74100) was focused onto the photovoltaic cell under test.

Synthesis. All chemicals were purchased from Aldrich and used without further purification. The structures of the monomers and polymer (Si-PCPDTTBT) are presented in Scheme 1.

1-Bromo-2-octanone (1). 2-Octanone (120 mL, 0.767 mol), urea (73.7 g, 1.23 mol), and glacial AcOH (375 mL) were placed in a 1000-mL round-bottom flask that was cooled in an ice bath. A solution of Br_2 (43 mL, 0.844 mmol) in glacial AcOH (120 mL) was added dropwise to the flask, and then the mixture was stirred overnight at room temperature. The mixture was poured into water (600 mL) and extracted with CH_2Cl_2; the organic phase was washed with 10% Na_2CO_3 and brine and then dried ($MgSO_4$). After evaporation of the solvent, the product was obtained through vacuum distillation (54.2 g, 34%). ^{1}H NMR: δ 3.88 (s, 2H), 2.62 (t, 2H), 1.58 (m, 2H), 1.35−1.15 (m, 6H), 0.86 (t, 3H). EI-MS: m/z 206.

4,4′-Dihexyl-2,2′-bithiazole (2). A mixture of **1** (14.6 g, 75.6 mmol), dithiooxamide (4.54 g, 37.8 mmol), and EtOH (190 mL) in a 250-mL round-bottom flask was heated under reflux for 24 h. After being allowed to cool, the mixture was poured onto crushed ice and extracted with CH_2Cl_2; the combined organic phases were then dried ($MgSO_4$). After evaporation of the solvent, the residue was purified chromatographically (SiO_2: EtOAc/hexane, 1:8) to give a light-brown oil (9.2 g, 39%). ^{1}H NMR: δ 6.92 (s, 2H), 2.76 (t, 4H), 1.72 (m, 4H), 1.40−1.15 (m, 12H), 0.86 (t, 6H). EI-MS: m/z 336.

5,5′-Dibromo-4,4′-dihexyl-2,2′-bithiazole (3). A mixture of **2** (8.00 g, 23.7 mmol) and *N*-bromosuccinimide (NBS, 10.7 g, 59.4 mmol) in glacial AcOH (80 mL) and dimethylformamide (DMF) (80 mL) was stirred for 2 h in the dark. The pale-yellow precipitate

was filtered off, washed with MeOH, and dried to give the dibromo product (6.0 g, 51%). ^{1}H NMR: δ 2.72 (t, 4H), 1.68 (m, 4H), 1.40−1.15 (m, 12H), 0.86 (t, 6H). EI-MS: m/z 492.

5,5′-Bis(2-thienyl)-4,4′-dihexyl-2,2′-bithiazole (4). Under an Ar atmosphere, a degassed solution of $NaHCO_3$ (0.85 g, 10 mmol) in water (ca. 46 mL) was added to a solution of **3** (1.0 g, 2.0 mmol), thiophen-2-ylboronic acid (0.73 g, 2.8 mmol), and $Pd(PPh_3)_4$ (0.047 g, 0.04 mmol) in THF (15 mL) at room temperature, and then the mixture was heated under reflux for 24 h. After the mixture had been cooled to room temperature, the organic solvent was evaporated under reduced pressure. The aqueous residue was extracted with CH_2Cl_2; the combined organic phases were then washed with water and brine, dried ($MgSO_4$), and concentrated under reduced pressure. The residue was reprecipitated with CH_2Cl_2/MeOH to give pale-yellow needles. ^{1}H NMR: δ 7.36 (d, 2H), 7.16 (d, 2H), 7.08 (t, 2H), 2.90 (t, 4H), 1.70 (m, 2H), 1,38−1.10 (m, 12H), 0.85 (t, 6H). EI-MS: m/z 500.

5,5′-Bis(5-bromo-2-thienyl)-4,4′-dihexyl-2,2′-bithiazole (5). NBS (0.52 g, 2.94 mmol) was added to a solution of **4** (0.70 g, 1.4 mmol) in $CHCl_3$ (7 mL) and glacial AcOH (1.75 mL), and then the mixture was stirred for 1 h in the dark. The precipitate was filtered off, washed with MeOH, and dried to give the dibromo product (0.6 g, 65%). ^{1}H NMR: δ 7.03 (d, 2H), 6.92 (d, 2H), 2.86 (t, 4H), 1.72 (m, 4H), 1.40−1.15 (m, 12H), 0.86 (t, 6H). EI-MS: m/z 656.

2,2′-Bithiophene (6) . 2-Bromothiophene (84 g, 510 mmol) was added dropwise to a suspension of Mg (12.6 g, 510 mmol) in dry THF (800 mL), and then the mixture was stirred at ambient temperature for 2 h. The resulting Grignard reagent was added dropwise to a mixture of 2-bromothiophene (84.0 g, 510 mmol) and Ni(dppp)Cl_2 (2.2 g, 5.0 mmol) in dry THF (700 mL) at 5−15 °C, and then the mixture was stirred at room temperature for 24 h. After evaporation of the solvent, the residue was purified chromatographically (SiO_2: hexane) to give the product (49 g, 72%) as a green solid. ^{1}H NMR: δ 7.19 (q, 4H), δ 7.01 (t, 2H).

3,3′,5,5′-Tetrabromo-2,2′-bithiophene (7). Br_2 (17.8 g, 111 mmol) was added dropwise over 1.5 h to a solution of **6** (5 g, 30 mmol) in glacial AcOH (20 mL) and $CHCl_3$ (45 mL) at 5−15 °C. The mixture was stirred at room temperature for 5 h and then under reflux for 24 h. After the mixture had been allowed to cool to room temperature, the reaction was quenched by adding aqueous KOH (10%, 50 mL). The aqueous phase was extracted with $CHCl_3$ (200 mL); the combined extracts were washed with water, dried ($MgSO_4$), filtered, and concentrated under reduced pressure. Recrystallization (EtOH) afforded off-white crystals (66%). ^{1}H NMR: δ 7.06 (s, 2H).

3,3′-Dibromo-5,5′-bis(trimethylsilyl)-2,2′-bithiophene (8). *n*-BuLi in hexane (1.6 M, 25 mL) was added dropwise over a period of 1 h to a solution of **7** (9.56 g, 20.0 mmol) in THF (300 mL) at −78 °C. The mixture was stirred for 15 min, chlorotrimethylsilane (5.4 g, 50 mmol) was added in one portion, and then the cooling bath was removed to warm the mixture to ambient temperature. The volatiles were evaporated under reduced pressure. The residue was purified chromatographically (SiO_2: hexane) to give a colorless oil (1.64 g, 18%). ^{1}H NMR: δ 7.04 (s, 2H), 0.33 (s, 18H). EI-MS: m/z 466.

4,4′-Bis(2-ethylhexyl)-5,5′-bis(trimethylsilyl)dithieno[3,2-b:2′,3′-d]silole (9). *n*-BuLi in hexane (1.6 M, 4.5 mL) was added dropwise over 5 min to a solution of **8** (1.6 g, 3.4 mmol) in THF (30 mL) at −78 °C. The mixture was stirred for 15 min, dichlorodi(2-ethylhexyl)silane (1.33 g, 4.00 mmol) was added in one portion, and then the cooling bath was removed, and the mixture was stirred for 2 h under ambient conditions. The mixture was then poured into water and extracted several times with Et_2O. The volatiles were evaporated under a vacuum, and the residue was purified chromatographically (SiO_2: hexane) to give a colorless oil (0.24 g, 12%). ^{1}H NMR: δ 7.06 (s, 2H), 1.72 (q, 2H), 1.52−1.14 (m, 16H), 0.92 (t, 6H), 0.86 (t, 6H), 0.76 (m, 4H), 0.32 (s, 18H). EI-MS: m/z 562.

4,4′-Bis(2-ethylhexyl)-5,5′-dibromodithieno[3,2-b:2′,3′-d]silole (10). NBS (3.8 g, 21 mmol) was added in one portion to a solution of **9** (5.8 g, 10 mmol) in THF (75 mL). After being stirred at ambient temperature for 4 h, the mixture was extracted with Et_2O, and the volatiles were evaporated under a vacuum. The residue was purified chromatographically (SiO_2: hexane) to give a yellow oil (5.3 g, 89%). ^{1}H NMR: δ 6.97 (s, 2H), 1.72 (q, 2H), 1.52−1.14 (m, 16H), 0.92 (t, 6H), 0.86 (t, 6H), 0.76 (m, 4H). EI-MS: m/z 574.

4,4′-Bis(2-ethyl-hexyl)-5,5′-bis(trimethyltin)-dithieno[3,2-b:2′,3′-d]silole (11). *n*-BuLi in hexane (1.6 M, 2.7 mL) was added dropwise to a solution of **10** (1.0 g, 1.7 mmol) in dry THF (30 mL) at −78 °C. After the mixture had been stirred for 15 min, trimethyltin chloride (1.0 g, 5.0 mmol) was added in one portion, and then the cooling bath was removed. The mixture was stirred at ambient temperature for 2 h and then poured into cool water and extracted several times with Et_2O. After evaporation of the volatiles, a sticky pale-green oil was obtained (1.2 g, 92%). ^{1}H NMR: δ 7.06 (s, 2H), 1.68 (m, 2H), 1.4−1.13 (m, 16H), 0.90 (t, 6H), 0.83 (t, 6H), 0.74 (m, 4H), 0.32 (s, 18H).

Poly[(4,4′-bis(2-ethylhexyl)dithieno[3,2-b:2′,3′-d]silole)-2,6-diyl-alt-(5,5′-thienyl-4,4′-dihexyl-2,2′-bithiazole)-2,6-diyl] (12). A solution of **5** (2.00 g, 2.68 mmol) and **11** (1.70 g, 2.68 mmol) in toluene (40 mL) was purged with Ar for 10 min, and then $Pd(PPh_3)_4$ (0.150 g, 0.134 mmol) and triphenylphosphine (0.21 g, 0.80 mmol) were added. After being purged with Ar for 20 min, the mixture was heated under reflux for 48 h in an oil bath set at 110 °C under an Ar atmosphere. The mixture was cooled to room temperature, MeOH (100 mL) was added, and the precipitated polymer was filtered off. After Soxhlet extraction with MeOH, hexane, and $CHCl_3$, the polymer was recovered from the $CHCl_3$ phase through reprecipitation with MeOH and then dried under a vacuum for 1 day (40%).

Fabrication of Solar Cell Devices. The polymer solar cells consisted of a layer of the Si-PCPDTTBT/PCBM blend thin film sandwiched between a transparent anode [indium tin oxide (ITO)] and a metal cathode. Prior to device fabrication, the ITO glasses (1.5 × 1.5 cm^2) were cleaned ultrasonically in detergent, deionized water, acetone, and isopropyl alcohol. After routine solvent cleaning, the substrates were treated with UV ozone for 15 min. The modified ITO surface was then obtained by spin-coating a layer of poly(3,4-ethylenedioxythiophene): poly(styrene sulfonate) (PEDOT:PSS) (ca. 30 nm). Subsequently, the active layer, Si-PCPDTTBT/PCBM (1:2, w/w), was spin-coated from dichlorobenzene (DCB) onto the PEDOT:PSS-modified ITO surface. Finally, layers of Ca (30 nm) and Al (100 nm) were thermally evaporated under a vacuum (pressure: $<6 \times 10^{-6}$ Torr) through a shadow mask. The active area of the device was 0.12 cm^2. In the hole-only devices, Ca was replaced with MoO_3 because its higher work function (Φ = 5.3 eV) provided a better hole injection contact for Si-PCPDTTBT/PCBM. The layer of MoO_3 was thermally evaporated to a thickness of 20 nm, and then it was capped with a layer of Al (50 nm). For the electron-only devices, the PEDOT:PSS layer

was replaced with $CsCO_3$ ($\Phi = 2.9$ eV), which is an efficient electron injection layer. This layer of Cs_2CO_3 was thermally evaporated to a thickness of 2 nm. The active layers were then annealed at 130 °C for 20 min to provide the final hole- and electron-only devices.

AUTHOR INFORMATION

Corresponding Author

*E-mail: gchu@gate.sinica.edu.tw. Telephone: +886-2-27898000 ext 70. Fax: +886-2-27826680.

ACKNOWLEDGMENT

The authors are grateful to the National Science Council (NSC), Taiwan (NSC 98-2221-E-001-002 and 99-2120-M-009-008), and Academia Sinica for financial support.

REFERENCES

(1) Huang, J. H.; Wei, H. Y.; Huang, K. C.; Chen, C. L.; Wang, R. R.; Chen, F. C.; Ho, K. C.; Chu, C. W. *Energy Environ. Sci.* **2010,** *3,* 654.
(2) Cha, H.; Kong, H.; Chung, D. S.; Yun, W. M.; An, T. K.; Hwang, J.; Kim, Y. H.; Shim, H. K.; Park, C. E. *Org. Electron.* **2010,** *11,* 1534.
(3) Wang, M.; Tang, Q.; An, J.; Xie, F.; Chen, J.; Zheng, S.; Wong, K. Y.; Miao, Q.; Xu, J. *ACS Appl. Mater. Interfaces* **2010,** *2,* 2699.
(4) de Bruyn, P.; Moet, D. J. D.; Blom, P. W. M. *Org. Electron.* **2010,** *11,* 1419.
(5) Seemann, A.; Egelhaaf, H. J.; Brabec, C. J.; Hauch, J. A. *Org. Electron.* **2009,** *10,* 1424.
(6) Blom, P. W. M.; Mihailetchi, V. D.; Koster, L. J. A.; Markov, D. E. *Adv. Funct. Mater.* **2007,** *19,* 1551.
(7) Tamayo, A.; Kent, T.; Tantitiwat, M.; Dante, M. A.; Rogers, J.; Nguyen, T. Q. *Energy Environ. Sci.* **2009,** *2,* 1180.
(8) Shoaee, S.; Eng, M. P.; Espildora, E.; Luis Delgado, J. L.; Campo, B.; Martin, N.; Vanderzande, D.; Durrant, J. R. *Energy Environ. Sci.* **2010,** *3,* 971.
(9) Siddiki, M. K.; Li, J.; Galipeau, D.; Qiao, Q. Q. *Energy Environ. Sci.* **2009,** *3,* 867.
(10) Padinger, F.; Rittberger, R. S.; Sariciftci, N. S. *Adv. Funct. Mater.* **2003,** *13,* 85.
(11) Kim, H.; Shin, M.; Kim, Y. *J. Phys. Chem. C* **2009,** *113,* 1620.
(12) Liu, Y.; Mills, E. N.; Composto, R. J. *J. Mater. Chem.* **2009,** *19,* 2704.
(13) Ko, C. J.; Lin, Y. K.; Chen, F. C. *Adv. Mater.* **2007,** *19,* 3520.
(14) Li, G.; Shrotriya, V.; Hunag, J.; Yao, Y.; Moriarty, T.; Emery, K.; Yang, Y. *Nat. Mater.* **2005,** *4,* 864.
(15) van Bavel, S. S.; Sourty, E.; de With, G.; Veenstrabd, S.; Loos, J. *J. Mater. Chem.* **2009,** *19,* 5388.
(16) Tang, H.; Lu, G.; Li, L.; Li, J.; Wang, Y.; Yang, X. *J. Mater. Chem.* **2010,** *20,* 683.
(17) Park, J. H.; Kim, J. S.; Lee, J. H.; Lee, W. H.; Cho, K. *J. Phys. Chem. C* **2009,** *113,* 17579.
(18) Peet, J.; Kim, J. Y.; Coates, N. E.; Ma, W. L.; Moses, D.; Heeger, A. J.; Bazan, G. C. *Nat. Mater.* **2007,** *6,* 497.
(19) Chen, H. Y.; Yang, H.; Yang, G.; Sista, S.; Zadoyan, R.; Li, G.; Yang, Y. *J. Phys. Chem. C* **2009,** *113,* 7946.
(20) Dante, M.; Garcia, A.; Nguyen, T. Q. *J. Phys. Chem. C* **2009,** *113,* 1596.
(21) Liu, J.; Shao, S.; Wang, H.; Zhao, K.; Xue, L.; Gao, X.; Xie, Z.; Han, Y. *Org. Electron.* **2010,** *11,* 775.
(22) Wang, E.; Wang, L.; Lan, L.; Luo, C.; Zhuang, W.; Peng, J.; Cao, Y. *Appl. Phys. Lett.* **2008,** *92,* 033307.
(23) Zhang, M.; Fan, H.; Guo, X.; He, Y.; Zhang, Z.; Min, J.; Zhang, J.; Zhan, G.; Li, Y. *Macromolecules* **2010,** *43,* 5706.
(24) Scharber, M. C.; Koppe, M.; Gao, J.; Cordella, F.; Loi, M. A.; Denk, P.; Morana, M.; Egelhaaf, H. J.; Forberich, K.; Dennler, G.; Gaudiana, R.; Waller, D.; Zhu, Z.; Shi, X.; Brabec, C. J. *Adv. Mater.* **2009,** *21,* 1.
(25) Chen, H. Y.; Hou, J.; Hayden, A. E.; Yang, H.; Houk, K. N.; Yang, Y. *Adv. Mater.* **2010,** *22,* 371.
(26) Huang, J. H.; Chien, F. C.; Kekuda, D.; Chen, P.; Ho, K. C.; Chu, C. W. *Anal. Chem.* **2010,** *82,* 1669.
(27) Huang, J. H.; Li, K. C.; Chien, F. C.; Hsiao, Y. S.; Kekuda, D.; Chen, P.; Lin, H. C.; Ho, K. C.; Chu, C. W. *J. Phys. Chem. C* **2010,** *114,* 9062.
(28) Li, K. C.; Huang, J. H.; Hsu, Y. C.; Huang, P. J.; Chu, C. W.; Lin, J. T.; Ho, K. C.; Wei, K. H.; Lin, H. C. *Macromolecules* **2009,** *42,* 3681.
(29) Chen, C. P.; Chan, S. H.; Chao, T. C.; Ting, C.; Ko, B. T. *J. Am. Chem. Soc.* **2008,** *130,* 12828.
(30) Ohshita, J. *Macromol. Chem. Phys.* **2009,** *210,* 1360.
(31) Viallat, A.; Born, R. P.; Cohen-Addad, J. P. *Polymer* **1994,** *35,* 2730.
(32) Veldman, D.; Ipek, Ö.; Meskers, S. C. J.; Sweelssen, J.; Koetse, M. M.; Veenstra, S. C.; Kroon, J. M.; van Bavel, S. S.; Loos, J.; Janssen, R. A. J. *J. Am. Chem. Soc.* **2008,** *130,* 7721.
(33) Heilemann, M.; Herten, D. P.; Heintzmann, R.; Cremer, C.; Müller, C.; Tinnefeld, P.; Weston, K. D.; Wolfrum, J.; Sauer, M. *Anal. Chem.* **2002,** *74,* 3511.
(34) Morana, M.; Azimi, H.; Dennler, G.; Egelhaaf, H. J.; Scharber, M.; Forberich, K.; Hauch, J.; Gaudiana, R.; Waller, D.; Zhu, Z.; Hingerl, K.; van Bavel, S. S.; Loss, J.; Brabec, C. J. *Adv. Funct. Mater.* **2010,** *20,* 1.
(35) Hoven, C. V.; Dang, X. D.; Coffin, R. C.; Peet, J.; Nguyen, T. Q.; Bazan, G. C. *Adv. Mater.* **2010,** *22,* 1.
(36) van Bavel, S. S.; Sourty, E.; de With, G.; Loos, J. *Nano Lett.* **2009,** *9,* 507.
(37) Yang, H.; Song, Q.; Lu, Z.; Guo, C.; Gong, C.; Hu, W.; Li, C. M. *Energy Environ. Sci.* **2010,** *3,* 1580.
(38) Huang, J. H.; Yang, C. Y.; Ho, Z. Y.; Kekuda, D.; Wu, M. C.; Chien, F. C.; Chen, P.; Chu, C. W.; Ho, K. C. *Org. Electron.* **2009,** *10,* 27.
(39) Melzer, C.; Koop, E. J.; Mihailetchi, V. D.; Blom, P. W. M. *Adv. Funct. Mater.* **2004,** *14,* 865.
(40) Mihailetchi, V. D.; Koster, L. J. A.; Blom, P. W. M.; Melzer, C.; de Boer, B.; van Duren, J. K. J.; Janssen, R. A. J. *Adv. Funct. Mater.* **2005,** *15,* 795.
(41) Li, G.; Yao, Y.; Yang, H.; Shrotriya, V.; Yang, G.; Yang, Y. *Adv. Funct. Mater.* **2007,** *17,* 1636.